Distal Site Aspartate Is Essential in the Catalase Activity of Catalase-Peroxidases†

Christa Jakopitsch,‡ Markus Auer,‡ Günther Regelsberger,‡ Walter Jantschko,‡ Paul Georg Furtmüller,‡ Florian Rüker,# and Christian Obinger*,‡

Institute of Chemistry and Institute of Applied Microbiology, University of Agricultural Sciences, Muthgasse 18, A-1190 Vienna, Austria

Received October 2, 2002; Revised Manuscript Received March 25, 2003

ABSTRACT: Structural and biochemical characterization of aspartate 152 at the distal heme side of catalase-peroxidase (KatG) from *Synechocystis* PCC 6803 reveals an important functional role for this residue. In the wild-type protein, the side chain carboxyl group of Asp152 is 7.8 Å apart from the heme iron and is hydrogen-bonded to two water molecules and a KatG-specific large loop. We have prepared the site-specific variants Asp152Asn, Asp152Ser, Asp152Trp, and Pro151Ala. Exchange of Asp152 exhibited dramatic consequences on the bifunctional activity of this unique peroxidase. The turnover number of catalase activity of Asp152Asn is 2.7%, Asp152Ser 5.7%, and Asp152Trp is 0.6% of wild-type activity. By contrast, the peroxidase activity of the Asp152 variants was 2−7 times higher than that of wild-type KatG or Pro151Ala. The KatG-specific pH profile of the catalase activity was completely different in these variants and exchange of Asp152 made it possible to follow the transition of the ferric enzyme to the redox intermediate compound I by hydrogen peroxide spectroscopically and to determine the corresponding bimolecular rate constant to be 7.5×10^6 M^{-1} s^{-1} (pH 7 and 15 °C). The reactivity of compound I toward aromatic one-electron donors was enhanced in the Asp152 variants compared with the wild-type protein, whereas the reactivity toward hydrogen peroxide was dramatically decreased. A mechanism for the hydrogen peroxide oxidation, which is different from monofunctional catalases and involves the distal residues Trp122 and Asp152, is proposed.

Catalase-peroxidases (KatGs)[1] are present in prokaryotes (archaebacteria and eubacteria) and fungi. On the basis of sequence similarities with yeast cytochrome *c* peroxidase (CCP) and plant ascorbate peroxidases (APXs), KatGs have been shown to be members of class I of the superfamily of plant, fungal, and bacterial heme peroxidases (*1*). Recently, the 2.0 Å crystal structure of the KatG from the archaebacterium *Haloarcula marismortui* has been published (*2*). It reveals that the enzyme is a dimer of two identical subunits. Each subunit is composed of two structurally homologous domains with a topology similar to that of either CCP or APX with heme *b* attached only to the N-terminal domain, formerly already ascribed to gene duplication (*3*). The arrangement of the catalytic residues is virtually identical in all class I peroxidases (*2*). In all members, the proximal heme pocket contains the amino acid triad His, Asp and Trp and the distal heme pocket the triad Trp, Arg, and His (Figure 1). The average differences for the coordinates of atoms in the heme *b* moiety and for both triads are 0.27 Å between CCP and *H. marismortui* KatG and 0.29 Å between APX and *H. marismortui* KatG (*2*). Interestingly, in the vicinity of the active site of KatG novel covalent bonds were proposed to be formed among the side chains of three residues including the conserved Trp (*2*). These covalent bonds seem to fix two long loops on the surface of the enzyme that cover the substrate access channel to the active site (*2*). It remains to demonstrate how these features contribute to the difference in the reactivities of class I peroxidases.

Catalase-peroxidases have a predominant catalase activity but differ from monofunctional catalases in also exhibiting a substantial peroxidatic activity with broad specificity. On the contrary, no substantial catalase activity has ever been reported for either CCP or APX. CCP is unusual in that it prefers another protein (cytochrome *c*) as a redox partner, whereas APXs prefer the anion ascorbate as electron donor. But both cytochrome *c* and ascorbate are poor substrates for KatGs (*4*−*6*).

Recently, the role of distal Trp, Arg, and His was studied in the KatGs from *Escherichia coli* (*7*, *8*) and from the cyanobacterium *Synechocystis* PCC 6803 (*8*, *9*). The data presented in these papers suggest that the distal His and Arg in KatGs have a role in the heterolytic cleavage of hydrogen peroxide (i.e., formation of the redox intermediate compound I) similar to other peroxidases (*10*). The distal Trp has been shown to be essential for H_2O_2 oxidation, i.e., the two-electron reduction step of compound I back to the ferric protein (*7*−*9*). The reasoning for this was based on the observations that in the Trp variants (i) the catalase activity was significantly reduced (*7*) or even lost (*8*, *9*), whereas (ii) the ratio of peroxidase to catalase activity was increased

† This work was supported by the Austrian Science Funds (FWF Project P15417).

* To whom correspondence should be addressed. Fax: 43−1−36006-6059. E-mail: christian.obinger@boku.ac.at.

‡ Institute of Chemistry.

Institute of Applied Microbiology.

[1] Abbreviations: KatG, catalase-peroxidase; APX, ascorbate peroxidase; CCP, cytochrome *c* peroxidase; HRP, horseradish peroxidase; CT1 (>600 nm), long wavelength porphyrin-to-metal charge-transfer band; POA, peroxoacetic acid.

10.1021/bi026944d CCC: $25.00
Published on Web 04/18/2003

(A)

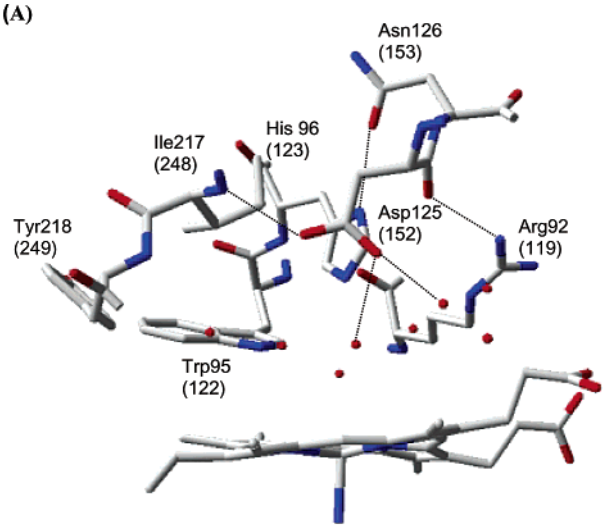

(B)

```
KatG_Syn6803 117 MIRMAWHAAGTYRIADGRGGAATGNQRFAPLNSWPDNVNLD 157
KatG_Halmar   90 FIRMAWHSAGTYRTADGRGGAAGGRQRFAPINSWPDNANLD 130
KatG_Myctub  102 FIRMAWHAAGTYRIHDGRGGAGGGMQRFAPLNSWPDNASLD 142
KatG_Esccol  100 FIRMAWHGAGTYRTYDGRGGASGGQQRFEPLNSWPDNVNLD 140
CCP_Saccer    46 LVRLAWHISGTWDKHDNTGGSYGGTYRFKKEFNDPSNAGLQ  86
APX_Pissat    36 ILRLAWHSAGTFDSKTKTGGPF-GTIKHQAELAHGANNGLD  75
```

FIGURE 1: Distal site structure of catalase-peroxidase from *H. marismortui*. The figure was constructed using the coordinates deposited in the Protein Data Bank (accession code 1ITK). The amino acid numbering is for *H. marismortui* KatG, but numbers in parentheses denote numbering for *Synechocystis* KatG. Only selected hydrogen bonds and water molecules (red) are shown. (B) Multiple sequence alignment performed for all three branches of class I peroxidases. Conserved active site residues are bold and the KatG-typical distal aspartate is in blue. KatG_Syn6803, catalase-peroxidase from *Synechocystis* PCC6803; KatG_Halmar; catalase-peroxidase from *H. marismortui*; KatG_Myctub, catalase-peroxidase from *Mycobacterium tuberculosis*; KatG_Esccol, catalase-peroxidase from *E. coli*; CCP_Saccer, cytochrome *c* peroxidase from *Saccharomyces cerevisiae*; APX_Pissat, ascorbate peroxidase from *Pisum sativum*.

dramatically (*7*, *8*), indicating that compound I formation was not influenced by this mutation.

Inspection of the active site of KatG from *H. marismortui* (*2*) shows an aspartate residue as part of the substrate entrance channel at the distal heme cavity. Its side chain carboxyl group (Asp125) is 7.81 Å from the heme iron and hydrogen-bonded to two water molecules, one being at a distance of 5.86 Å from the ferric atom (Figure 1A). Sequence alignments reveal that this residue is conserved in all KatGs analyzed so far (Figure 1B). In *Synechocystis* KatG, this residue is Asp152 and, as modeling has demonstrated, in a very similar position (not shown). Interestingly, neither in cytochrome *c* peroxidase nor in ascorbate peroxidase this residue is found.

In KatGs, this Asp is part of the triad Pro−Asp−Asn (in *Synechocystis* KatG Pro151−Asp152−Asn153), whereas in CCP a serine substitutes the aspartate forming the triad Pro80−Ser81−Asn82 and in APX an alanine substitutes the aspartate giving the triad Gly69−Ala70−Asn71, respectively (Figure 1B). The neighboring Asn [Asn126 in *H. marismortui* KatG (Figure 1A) and Asn153 in *Synechocystis* KatG] is hydrogen-bonded to the distal histidine (*2*). This His−Asn couple is conserved in all plant-type peroxidases (*10*).

In this work, Asp152 of KatG from *Synechocystis* PCC 6803 was replaced with Asn (Asp152Asn), Ser (Asp152Ser), and Trp (Asp152Trp). In addition, substitution of Pro151 by Ala (an adjoining residue that is not involved in the catalytic mechanism) was performed to estimate the impact of mutation on the proper folding and reactivity of the recombinant protein. A comprehensive steady-state and transient-state kinetic analysis was performed demonstrating an important role of the distal Asp in the KatG-specific hydrogen peroxide oxidation reaction. The Asp152 variants exhibited a dramatically reduced catalase activity but an increased peroxidase activity. The consequence was that compound I formation and reduction with hydrogen peroxide could be followed spectroscopically. A novel mechanism of H_2O_2 oxidation, which is different from monofunctional catalases and includes distal Trp122 and Asp152 is proposed.

MATERIALS AND METHODS

Reagents. Standard chemicals and biochemicals were obtained from Sigma Chemical Co. at the highest grade available. Expression, purification of KatGs from *Synechocystis*, and spectrophotometric characterization of wild type and mutant proteins were described previously (*9*).

Mutagenesis. Oligonucleotide site-directed mutagenesis was performed using PCR-mediated introduction of silent mutations as described (*9*). A pET-3a expression vector that contained the cloned catalase-peroxidase gene from the cyanobacterium *Synechocystis* PCC 6803 (*5*, *9*) was used as the template for PCR. At first, unique restriction sites were selected flanking the region to be mutated. The flanking primers were 5′-AAT GAT CAG GTA CCG GCC AGT AAA TG-3′ containing a *Kpn*I restriction site and 5′-TGC ATA AAG GAT CCG GGT GC-3′ containing a *Bam*HI restriction site. The internal 3′-primer was 5′-CCA GGA ATT CAG GGG GGC GAA GC-3′ and possessed a *Eco*RI restriction site. The following mutant primers with the desired mutation and a silent mutation introducing a restriction site were constructed (point mutations italicized and restriction sites underlined): 5′-CCC CCT GAA T*TC* CTG GCC A*A*A TAA CGT CAA TTT AGAC-3′ changed Asp152 to Asn; 5′-CTG AAT *TC*C TGG CCA *TC*T AAC GTC AAT TTA GAC-3′ changed Asp152 to Ser; 5′-CTG AAT *TC*C TGG CCA *TGG* AAC GTC AAT TTA GAC-3′ changed Asp152 to Trp; 5′-CCT GAA T*TC* CTG G*G*C AGA TAA CGT C-3′ changed Pro151 to Ala. The fragment defined by the *Kpn*I and *Bam*HI restriction sites was replaced by the new construct containing the point mutation. All constructs were sequenced to verify DNA changes using thermal cycle sequencing.

Spectroscopic Studies. Optical spectra were recorded on a diode array spectrophotometer (Zeiss Specord S10) and a Hitachi U-3000 spectrophotometer equipped with a thermostated cell holder. Circular dichroism studies were carried out using a JASCO J-600 spectropolarimeter. Far-UV (190−260 nm) experiments were carried out using protein concentrations of 1.5 μM, and the path length of the cuvette was 1 mm. A good signal-to-noise ratio in the CD spectra was obtained by averaging 12 scans (resolution: 1 nm; bandwidth: 1 nm; response 16 s; scan speed 20 nm/min).

Steady-State Kinetics. Peroxidase activity was monitored spectrophotometrically using 1 mM H_2O_2 and 5 mM guaiacol (ϵ_{470} = 26.6 mM^{-1} cm^{-1}) or 1 mM *o*-dianisidine (ϵ_{460} = 11.3 mM^{-1} cm^{-1}). Peroxidase activity with pyrogallol was

monitored using 100 μM H_2O_2 and 20 mM pyrogallol (ϵ_{430} = 2.47 mM^{-1} cm^{-1}). One unit of peroxidase is defined as the amount that decomposes 1 μmol of electron donor/min at pH 7 and 30 °C.

Catalase activity was determined polarographically in 50 mM phosphate buffer using a Clark-type electrode (YSI 5331 Oxygen Probe) inserted into a stirred water bath (YSI 5301B) at 30 °C. Alternatively, the catalase activity was measured by continuously monitoring hydrogen peroxide concentration polarographically with a platinum electrode covered with a hydrophilic membrane and fitted to the Amperometric Biosensor Detector 3001 (Universal Sensors, Inc., USA). The applied electrode potential at pH 7 was 650 mV and the H_2O_2 electrode filling solution was prepared freshly half-daily. The electrode was calibrated against known concentrations of hydrogen peroxide. All reactions were performed at 30 °C and started by the addition of KatG. One unit of catalase is defined as the amount that decomposes 1 μmol of H_2O_2/min at pH 7 and 30 °C. To cover the pH range 4−9, 50 mM citrate−phosphate or 50 mM Tris/HCl buffers were used. Since the potential of hydrogen peroxide increases with decreasing pH the applied electrode potential had to be changed from 890 mV (pH 4) to 530 mV (pH 9).

Transient-State Kinetics. Transient-state measurements and calculation of pseudo-first-order rate constants (k_{obs}) from experimental traces were performed as described earlier (*8*, *9*). The kinetics of oxidation of ferric catalase-peroxidase to compound I by peroxoacetic acid, *m*-chloroperoxybenzoic acid, or hydrogen peroxide or the formation of the cyanide complex were followed in the single mixing mode. Catalase-peroxidase and the peroxide or cyanide were mixed to give a final concentration of 1 μM enzyme and 5−250 μM peroxide or 20−500 μM cyanide. Sequential-mixing stopped-flow analysis was used to measure compound I reduction by one-electron donors. In the first step, the enzyme was mixed with peroxoacetic acid or H_2O_2 and, after a delay time where compound I was built, the intermediate was mixed with the electron donors aniline, ascorbate, or *o*-dianisidine. All stopped-flow determinations were measured in 50 mM phosphate buffer, pH 7.0 and 15 °C, and at least three determinations were performed per substrate concentration.

RESULTS

Spectral Properties. Figure 2A depicts the UV−Vis spectra of wild-type KatG and the four variants investigated in this study. The spectra of Asp152Asn and Asp152Ser were similar to that of the recombinant wild-type enzyme in the resting state exhibiting the typical bands of a heme *b*-containing peroxidase in the visible and near-ultraviolet region (*5*, *8*, *9*), whereas Asp152Trp and Pro151Ala showed some deviations at the Soret band and in the visible region, respectively. A Soret peak at 406 nm (small shoulder at 380 nm) together with two bands around 500 and 635 nm (CT1) in the spectrum of wild type *Synechocystis* KatG suggest the presence of a dominating five-coordinate high-spin heme coexisting with some six-coordinate high-spin heme (*11*). The Soret band of the Asp152 variants was at 405 nm and the CT1 band slightly red-shifted to 642 nm (Asp152Asn), 640 nm (Asp152Ser), and 638 nm (Asp152Trp), respectively. The A_{406}/A_{280} ratios (i.e., Reinheitszahl) were 0.42−0.44 (Asp152Asn), 0.40−0.43 (Asp152Ser), 0.49−0.52 (Asp152Trp), and 0.36−0.38 (Pro151Ala) with small variations from one preparation to another (wild-type protein: 0.57−0.61). In Asp152Trp, the shoulder at 368 nm indicated the presence of some free heme.

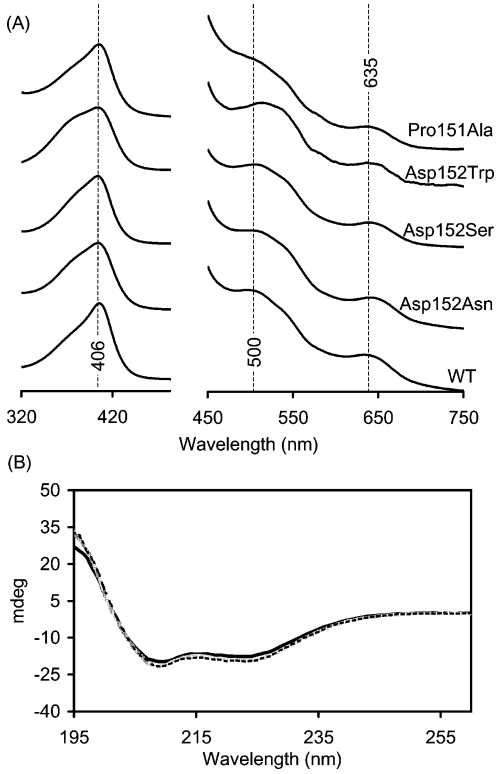

FIGURE 2: UV−Vis spectra and circular dichroism spectra of the ferric forms of wild-type KatG and variants. (A) UV−Vis spectra of *Synechocystis* wild type (WT) KatG and of the variants Asp152Ser and Asp152Trp and Pro151Ala. Proteins in 50 mM phosphate buffer, pH 7.0 and 25 °C. The absorbance ratio (A_{Soret}/A_{280}) of the proteins was 0.60 for wild-type KatG, 0.43 for Asp152Asn, 0.41 for Asp153Ser, 0.50 for Asp152Trp, and 0.37 for Pro151Ala, respectively. The region between 450 and 750 nm has been expanded 6-fold. (B) Circular dichroism spectra of wild-type KatG (bold line) and the variants Asp152Ser (dotted line) and Asp152Trp (grey line). Conditions: Ferric proteins (1.5 μM) in 10 mM phosphate buffer, pH 7.0 and 25 °C.

The CD spectra of wild type KatG and the variants (Figure 2B) are characteristic of a protein composed primarily of α helices. Very little difference was observed between wild-type KatG and the variants. If conformational changes did occur, they must have been very localized and minimal and thus went undetected by CD.

The protein yield was 60−80 mg of recombinant KatG from 1 L of *E. coli* culture for the Asp variants and 20−25 mg for Pro151Ala.

Catalase and Peroxidase Activity. Recombinant wild type KatG exhibits an overwhelming catalase activity. The polarographically measured specific catalase activity in the presence of 5 mM hydrogen peroxide is (1160 ± 55) units/mg of protein. All Asp152 variants exhibited a dramatically reduced catalase activity (Table 1). Compared with wild-type KatG the k_{cat} values of Asp152Asn, Asp152Ser, and Asp152Trp were determined to be 2.7, 5.7, and 0.6%, respectively. By contrast, the overall peroxidase activity of the Asp152 variants was 2−7 times higher than that of wild type *Synechocystis* KatG (Table 1). Mutation of Pro151 had only minor effects on the bifunctional activity of this enzyme.

Table 1: Apparent K_m and k_{cat} Values for the Catalase Activity of Wild Type and Variant Catalase-Peroxidase from *Synechocystis* PCC 6803,[a] and Specific Peroxidase Activities[b]

	catalase activity			peroxidase activity (units mg^{-1})		
	K_m (mM)	k_{cat} (s^{-1})	k_{cat}/K_m ($\times 10^5$ M^{-1} s^{-1})	pyrogallol	*o*-dianisidine	guaiacol
wild type	4.1 ± 0.2	3500 ± 350	8.5	6.6 ± 0.4	3.2 ± 0.3	0.6 ± 0.1
Asp152Asn	2.5 ± 0.1	95 ± 9	0.4	12.5 ± 0.4	7.5 ± 0.4	2.5 ± 0.1
Asp152Ser	2.4 ± 0.2	200 ± 25	0.8	13.6 ± 0.5	7.6 ± 0.4	2.5 ± 0.2
Asp152Trp	3.2 ± 0.3	20 ± 4	0.06	7.3 ± 0.5	21.5 ± 0.1	4.1 ± 0.2
Pro151Ala	2.5 ± 0.1	2500 ± 190	10.4	4.1 ± 0.1	2.4 ± 0.2	0.5 ± 0.1

[a]Reaction conditions: 50 mM phosphate buffer, pH 7 and 30 °C. For catalase and peroxidase assays as well as unit definition see Materials and Methods. [b] Units per milligram of protein.

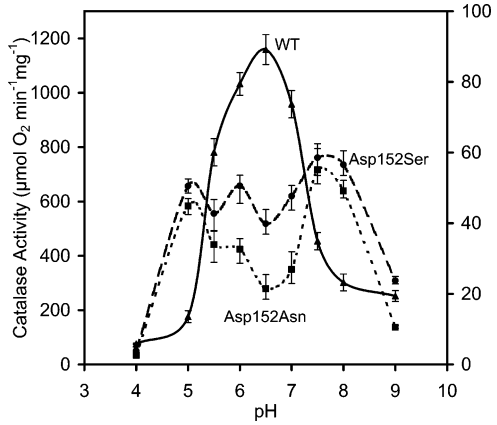

FIGURE 3: pH profile for the catalase activity of *Synechocystis* catalase-peroxidase. The specific catalase activity of wild type (WT) KatG and the variants Asp152Asn and Asp152Ser is given in μmoles of O_2 formed per minute and milligram of protein as determined polarographically at 30 °C in 50 mM citrate−phosphate or Tris buffers, pH 4.0−9.0. Note that for both variants the right *y*-axis is valid.

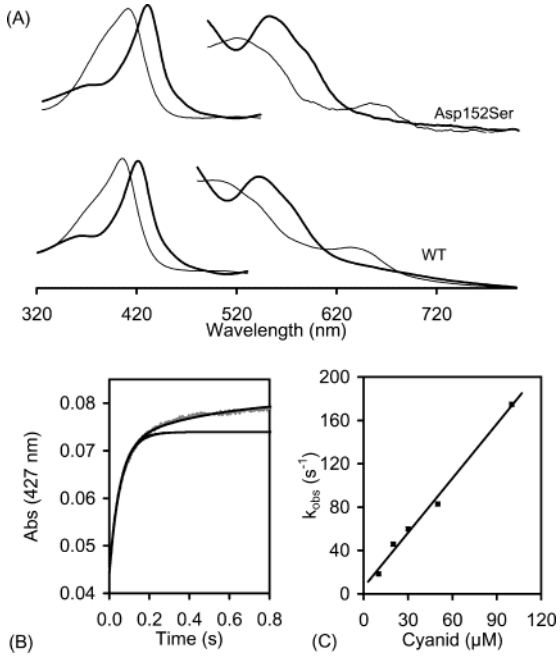

FIGURE 4: Cyanide binding to the ferric forms of *Synechocystis* wild type (WT) KatG and Asp152Ser. (A) UV−Vis spectra of the ferric forms and cyanide complexes (bold) of *Synechocystis* wild-type KatG and Asp152Ser. Conditions: Ferric proteins (2 μM) were mixed with 10 mM cyanide in 50 mM phosphate buffer, pH 7.0 and 25 °C. The region between 500 and 800 nm has been expanded 6-fold. (B) Typical time trace (grey line) and fits (single and double exponential) of the reaction between Asp152Ser (1 μM) and 10 μM cyanide followed at 427 nm in 50 mM phosphate buffer, pH 7.0 and 15 °C. (C) Pseudo-first-order rate constants for the formation of the cyanide complex of Asp152Ser in 50 mM phosphate buffer, pH 7.0 and 15 °C.

Most interesting was the finding that the KatG-specific pH profile of the catalase activity (i.e., maximum activity around pH 6.5) was completely different in the Asp152 variants. In Asp152Ser, the specific catalase activity did not change in the region pH 5−8, and in Asp152Asn even a minimum was found at pH 6.5 (Figure 3). These results, found by both following oxygen evolution using a Clark-type electrode or hydrogen peroxide depletion using a hydrogen peroxide electrode, suggest a prominent role of distal Asp in the hydrogen peroxide oxidation reaction of catalase-peroxidases. By contrast, the pH dependence of Pro151Ala was similar to that of wild-type KatG.

Cyanide Binding. Cyanide is a useful probe to investigate the binding site of heme proteins. Figure 4A shows the spectral changes upon addition of cyanide to ferric wild-type KatG and Asp152Ser. A similar low spin spectrum was obtained when the other variants were mixed with excess cyanide (not shown). The Soret peak shifted to 422 nm (isosbestic point at 414 nm) and a prominent new peak around 540 nm was seen. In case of wild-type KatG, the shift of the Soret peak was accompanied by a small hypochromicity, whereas in case of the Asp152 variants a small hyperchromicity was observed. Cyanide binding was monophasic in case of wild-type KatG and Pro151Ala and gave single-exponential curves, indicating pseudo-first-order kinetics. Cyanide binding to the Asp152 variants was biphasic with a rapid first phase responsible for about 85% of the absorbance increase at 427 nm (the wavelength at maximum absorbance difference between the cyanide complex and the ferric protein). A typical time trace for the reaction of Asp152Ser with cyanide followed at 427 nm is shown in Figure 4B including a single and double exponential fit. Fitting the first rapid phase by using a single-exponential equation or using the dominating exponential term of the double exponential equation gave similar results. The obtained pseudo-first-order rate constants, k_{obs}, showed that with all variants the k_{obs} values linearly increased with the concentration of cyanide (Figure 4C). The slope yielded the apparent second-order rate constant for cyanide binding (k_{on}). The value obtained for the wild-type enzyme is (4.8 ± 0.4) $\times 10^5$ M^{-1} s^{-1} at pH 7 and 15 °C. The finite intercept (7.6 s^{-1}) represents k_{off}. From the ratio k_{off}/k_{on}, a value for the dissociation constant of the cyanide complex to ferric enzyme and cyanide of 15.8 μM was calculated. A similar binding rate was found with the Pro151 variant (Table 2). However, cyanide binding to the Asp152 variants

Table 2: Bimolecular Rate Constants of Compound I Formation, Cyanide Binding, and Compound I Reduction for Wild Type *Synechocystis* PCC 6803 Catalase-Peroxidase and the Variants Asp152Asn, Asp152Ser, Asp152Trp, and Pro151Ala[a]

reaction	substrate	wild type ($\times 10^4$ M^{-1} s^{-1})	Asp152Asn ($\times 10^4$ M^{-1} s^{-1})	Asp152Ser ($\times 10^4$ M^{-1} s^{-1})	Asp152Trp ($\times 10^4$ M^{-1} s^{-1})	Pro151Ala ($\times 10^4$ M^{-1} s^{-1})
compound I formation	peroxoacetic acid	3.9 ± 0.4	37 ± 6	26 ± 5	34 ± 7	3.3 ± 0.4
	m-CPB	5.3 ± 0.5	610 ± 35	170 ± 30	910 ± 45	2.8 ± 0.4
	hydrogen peroxide	n.d.	750 ± 40	750 ± 35	450 ± 30	n.d.
cyanide binding	cyanide	48 ± 4	95 ± 5	170 ± 15	135 ± 20	45 ± 3
compound I reduction[A]	pyrogallol	8.6 ± 0.5	166 ± 45	160 ± 30	−	33 ± 6
	ascorbate	0.7 ± 0.05	1.3 ± 0.1	0.9 ± 0.05	−	0.4 ± 0.05
	o-dianisidine	271 ± 35	n.d.	n.d.	−	570 ± 50
compound I reduction[B]	pyrogallol	n.d.	270 ± 35	280 ± 30	−	n.d.
	ascorbate	n.d.	0.9 ± 0.1	0.8 ± 0.05	−	n.d.
	o-dianisidine	n.d.	n.d.	n.d.	−	n.d.

[a] Conditions: 50 mM phosphate buffer, pH 7.0 and 15 °C. Compound I was formed with either peroxoacetic acid[A] or hydrogen peroxide.[B] For details, see Materials and Methods. n.d., not detectable; −, not determined.

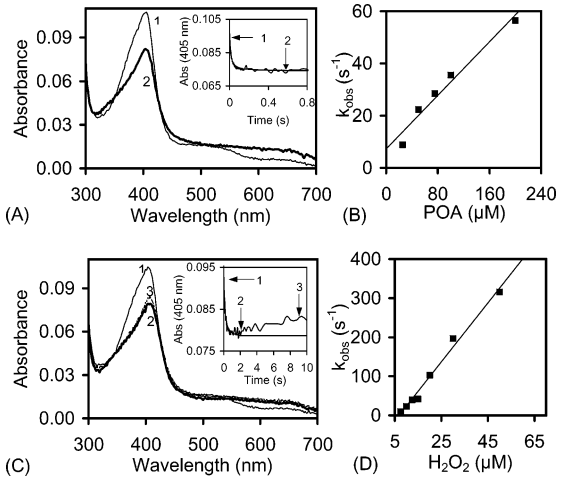

FIGURE 5: Compound I formation of the *Synechocystis* KatG variants Asp152Ser and Asp152Asn. (A) Spectral changes upon addition of peroxoacetic acid to ferric Asp152Ser. Final concentrations: 100 μM peroxoacetic acid and 1 μM Asp152Ser. First spectrum is that of ferric enzyme. Second spectrum (bold) is that of compound I and was taken after 600 ms. The inset shows the corresponding time trace and fit (405 nm; 50 mM phosphate buffer, pH 7.0 and 15 °C). (B) Pseudo-first-order rate constants for the formation of Asp152Ser compound I plotted against peroxoacetic acid (POA) concentration. (C) Spectral changes upon addition of hydrogen peroxide to ferric Asp152Asn. Final concentrations: 50 μM H_2O_2 and 1 μM ferric Asp152Asn in 50 mM phosphate buffer, pH 7.0, at 15 °C. First spectrum (1) is that of ferric enzyme. Second spectrum (bold, 2) was taken after 2 s, and the third spectrum (dotted line, 3) was taken after 10 s. The inset shows the corresponding time trace at 405 nm and the double-exponential fit of the reaction described in (C) with the numbers indicating times of spectrum selection. (D) Pseudo-first-order rate constants for the formation of Asp152Asn compound I plotted against hydrogen peroxide concentration.

was faster (Table 2) and the corresponding calculated dissociation constants were decreased [Asp152Asn: 2.4 μM; Asp152Ser: 4.3 μM; Asp152Trp: 5.8 μM).

Compound I Formation. As has been reported recently, the catalase activity of wild-type KatGs does not allow one to follow compound I formation by addition of hydrogen peroxide (*4*, *5*, *9*). However, upon addition of peroxoacetic acid a compound I spectrum can be obtained that is distinguished from the resting state by a 40−50% hypochromicity, and its formation can be followed as exponential absorbance decrease at the Soret maximum. This is also the case for the Asp152 variants (Figure 5A). Depending on the variant the isosbestic points of this spectral transition varied between 354 and 355 nm and 428−430 nm and the maximum hypochromicity at the Soret band was 30−35%. With an excess of peroxoacetic acid single-exponential time traces were obtained (inset to Figure 5A) and the plots of the pseudo-first-order rate constants, k_{obs}, versus peroxoacetic acid concentration were linear (Figure 5B), allowing the calculation of the bimolecular rate constants (k_1) from the slope. As Table 2 shows, peroxoacetic acid mediated compound I formation of the Asp152 variants was about 1 order of magnitude faster than that of wild-type KatG. With *m*-chloroperbenzoic acid as oxidant, the rates of compound I formation were increased even by factors of 30−170 (Table 2). By contrast, the kinetics of the Pro151Ala variant were similar to that of wild-type KatG.

Interestingly, the Asp152 variants also allowed us to follow spectral changes mediated by hydrogen peroxide. This, besides the altered pH dependence, gives further strong evidence for an important role of the distal aspartate in the H_2O_2 oxidation reaction. Figure 5C shows the spectral changes and kinetics of the reaction between 1 μM Asp152Asn and 50 μM H_2O_2. A hypochromicity of about 25% was observed and the isosbestic points at 353 and 428 nm indicate formation of a compound I-like intermediate or at least of the dominating steady-state spectrum during the catalase turnover. Depending on the added amount of hydrogen peroxide, a re-increase of the absorbance at the Soret band was observed (inset to Figure 5C). Finally, the spectrum of the ferric protein is reestablished (which corresponds to the complete degradation of hydrogen peroxide). Fitting of the H_2O_2 mediated absorbance decrease at the Soret peak was best by using a double-exponential equation (inset to Figure 5C). Similar results were obtained by either fitting the first rapid phase to a single-exponential equation or by taking the k_{obs} values from the dominating exponential term in the double exponential fit and by plotting these parameters versus the concentration of hydrogen peroxide (Figure 5D). The calculated rate constants (k_1) varied between $(4.5 \pm 0.3) \times 10^6$ M^{-1} s^{-1} (Asp152Trp) and $(7.5 \pm 0.4) \times 10^6$ M^{-1} s^{-1} (Asp152Ser) (Table 2).

The possibility to use both peroxoacetic acid and H_2O_2 in compound I formation allowed the estimation of the concentration of compound I during the catalatic steady-state by assuming that with peroxoacetic acid 100% compound I is obtained, whereas the resulting spectrum with H_2O_2 represents the catalatic steady-state. The concentration of compound I during steady-state is determined by the ratio

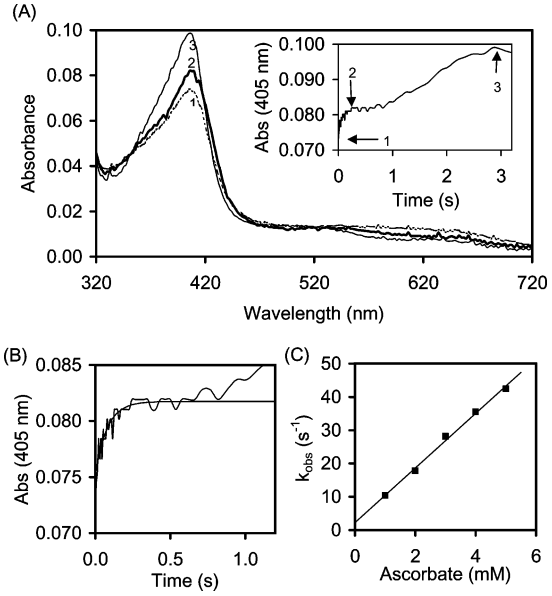

FIGURE 6: Compound I reduction of the *Synechocystis* KatG variant Asp152Ser. (A) Spectral changes upon addition of ascorbate to Asp152Ser compound I formed with hydrogen peroxide. Final concentrations: 1 μM Asp152Ser compound I and 2 mM ascorbate. First spectrum (1, dotted line) is that of Asp152Ser compound I taken 12.8 ms after adding ascorbate. Second spectrum (2, bold) is taken after 100 ms, and third spectrum (3) is taken after 3 s. The inset shows the corresponding time trace at 405 nm and 15 °C (50 mM phosphate buffer, pH 7.0) with numbers indicating times of spectrum selection. (B) Time trace (405 nm) and single-exponential fit of compound II formation. 1 μM of compound I formed with hydrogen peroxide was mixed with 2 mM ascorbate (50 mM phosphate buffer, pH 7.0 and 15 °C). (C) Pseudo-first-order rate constants for Asp152Asn compound I reduction plotted against ascorbate concentration.

of the rate of compound I formation (k_1) to that of compound I reduction (k_2). Analysis of the corresponding spectra show that in the catalatic steady-state compound I is dominating (86−88% in Asp152Ser and 91−93% in Asp152Asn), demonstrating that $k_1 > k_2$, which is in strong contrast to wild-type KatG or Pro151Ala ($k_2 \gg k_1$), thus underling the important role of Asp152 in compound I reduction.

Independently of the oxidant used in oxidation of the ferric proteins, the formed redox intermediate allowed us to study its reactivity with electron donors using the sequential-mixing stopped-flow technique.

Compound I Reduction. In a typical experiment, 4 μM recombinant protein was premixed in the aging loop with 200 μM peroxoacetic acid or 200 μM hydrogen peroxide, and after a delay time of 3 or 2 s (in case of H_2O_2), the electron donor was added. Similar to earlier observations with wild-type KatG (*4*, *5*), distal (*8*, *9*) and proximal mutants (*12*), addition of classical one-electron donors to compound I resulted in the formation of a redox intermediate with spectral features that did not resemble a typical (red-shifted) compound II spectrum known from other peroxidases (e.g., horseradish peroxidase or APX). The Soret band remained at 405 nm, with the extinction coefficient being between that of compound I and the ferric protein (Figure 6A). Consequently, compound I reduction of the Asp152 variants has been followed at 405 nm. A typical time trace with ascorbate as electron donor is shown in the inset of Figure 6A. Inspection of the time trace showed that the reaction is biphasic exhibiting an exponential increase (which could be attributed to compound II formation) followed by a slow conversion back to the ferric enzyme. The slow phase fits well with the observation that ascorbate is general a very poor substrate of KatGs. To obtain actual bimolecular rate constants (which could represent the one-electron reduction of compound I to compound II) the first exponential phase was fitted (Figure 6B) and the pseudo-first-order rate constants were plotted against the electron donor concentration (Figure 6C). The obtained data (summarized in Table 2) show unequivocally that mutation of Asp152 in *Synechocystis* KatG did not change the hierarchy in reactivity toward the three investigated electron donors (ascorbate < pyrogallol ≪ *o*-dianisidine). However, the calculated rates of compound I reduction by the aromatic substrates were enhanced by more than 1 order of magnitude. In case of pyrogallol the reaction was 18 times faster with Asp152Asn and Asp152Ser compared to wild-type KatG, and in case of *o*-dianisidine it was even too fast to monitor. By contrast, the reactivity toward ascorbate did not change upon mutation. As Table 2 shows similar results were obtained independent of the peroxide used for compound I formation.

DISCUSSION

Catalase-peroxidases are unique members in the superfamily of plant, fungal, and prokaryotic peroxidases. Though having a peroxidase-typical heme site architecture, they are capable of performing a catalase activity similar to that of monofunctional catalases which, however, have both different heme cavity residues as well as three-dimensional structures.

Principally, the organization of the active site of catalase-peroxidases is similar to that of the homologous peroxidases CCP (*13*) and APX (*14*) (Figure 1). Even the coordinates of the distal Trp, which has recently been shown to be essential in the catalase activity of KatGs (*7*, *8*), agree with that of CCP and APX, but both cannot oxidize H_2O_2. One important difference becomes evident from inspection of the recently published first 3D structure of a KatG (*2*). This structure as well as the alignment of all KatG genes sequenced so far clearly show the presence of an aspartate residue at the distal heme side with its carboxylate group being at a distance of 7.8 Å from the heme iron (Figure 1A). The corresponding residues in CCP and APX are Ser and Ala, respectively (Figure 1B). The backbone atoms of these residues overlap (not shown), but the negatively charged carboxylate group of Asp in KatG is a prominent part of the distal heme cavity, whereas the hydroxyl group of Ser in CCP points away (*13*). In the *H. marismortui* KatG structure (*2*), the distance between the carboxylate oxygen atoms and N_ϵ of the distal His is 4.6 and 4.8 Å, respectively, and the distance between the carboxylate oxygens and the indole nitrogen of Trp is 6.8 and 7.38 Å, respectively.

Besides its important role in the hydrogen peroxide oxidation reaction (see below and Figure 7) the distal aspartate plays a role in the stabilization of a KatG-specific large loop (named LL1 in the recently published *H. marismortui* KatG structure). In Figure 1, this loop-stabilizing hydrogen bond between Asp152 and Ile248 (*Synechocystis* numbering) is shown. It is interesting to note that Ile248 is the immediate neighbor of Tyr249 which has been proposed to be covalently linked via its $C_\epsilon 1$ to the $C_\eta 2$ of distal Trp122 (*2*). Both Ile248 and Tyr249 are part of this KatG-specific

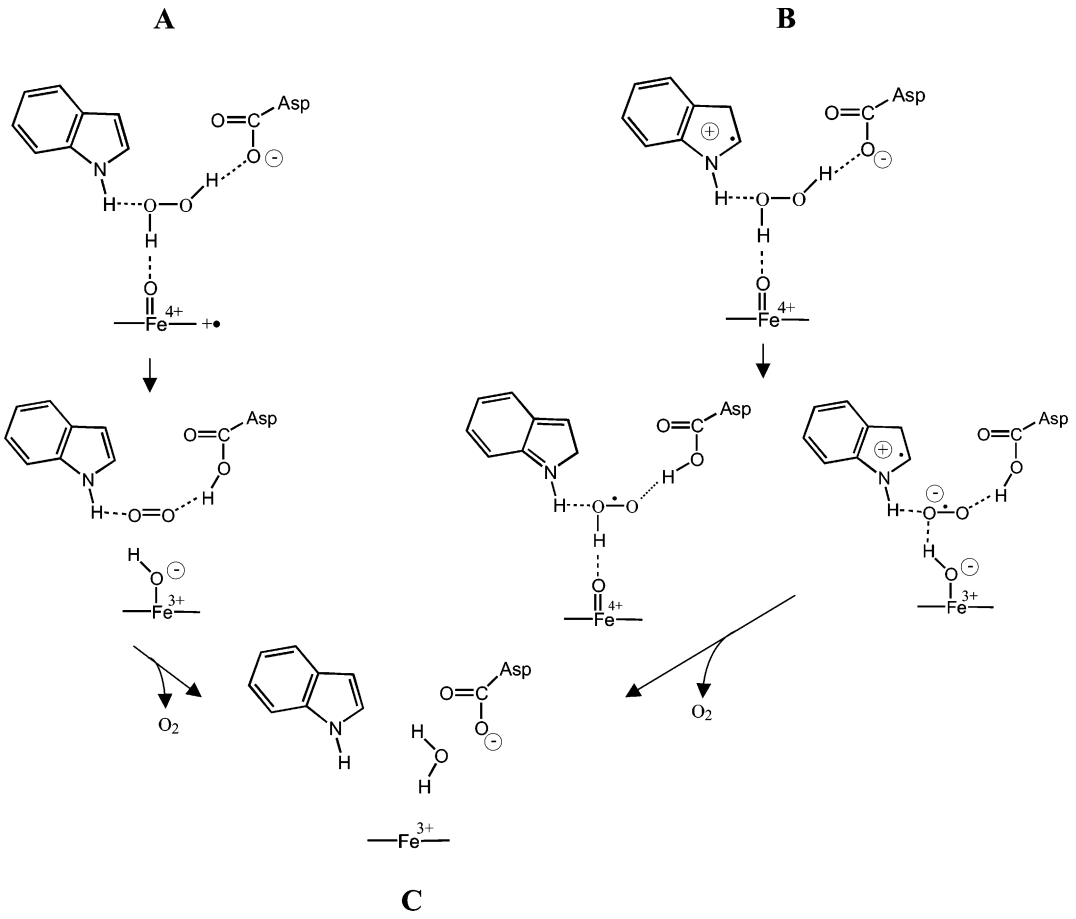

FIGURE 7: Hypothetical pathways of hydrogen peroxide oxidation by catalase-peroxidase compound I. Left pathway: Reduction of compound I (A: oxyferryl plus porphyrin radical) to ferric KatG (C) involving a pairwise movement of electrons producing singlet oxygen. Right pathway: Reduction of compound I (B: oxyferryl plus protein radical) involving two one-electron-transfer steps releasing triplet oxygen.

loop LL1. Together with a second KatG-specific loop (LL2) at the opposite heme edge (*2*) LL1 is part of a small narrow substrate channel with a length of about 20 Å. In addition, main chain carbonyl group of Asp152 is (as are the corresponding residues in CCP and APX) hydrogen bonded to the peroxidase-typical arginine (Arg119 in *Synechocystis* KatG) (Figure 1).

Recent spectral UV−Vis and resonance Raman studies of KatG variants (exchanges of distal Trp or His or Arg) showed that the charge at the distal side of KatG is important for maintaining the heme architecture (*11*). In contrast to corresponding CCP (*15*) and HRP (*16*) mutants, the *Synechocystis* KatG variants Arg119Ala and His123Glu were shown to be very unstable, easily losing the prosthetic group even at neutral pH (*11*). This led to the conclusion that a negatively charged residue in the distal cavity destabilizes the heme pocket (*11*).

The present work for the first time gives strong evidence for an essential role of the KatG-typical distal aspartate in the bifunctional activity of catalase-peroxidases. Together with previous data on engineered KatGs (*7*−*9*, *12*), we can now postulate a mechanism for both reaction steps in the catalase activity of a KatG, namely, for hydrogen peroxide reduction and hydrogen peroxide oxidation. Different residues are involved in these reactions. Similar to other members of the plant peroxidase superfamily, the amino acid couple His−Arg is important in the heterolytic cleavage of hydrogen peroxide forming the redox intermediate compound I which is common to both the catalatic and the peroxidatic cycle. A mechanism as proposed by Poulos and Kraut (*17*) applies also to KatGs, since exchange of distal His or Arg in KatG influenced the overall catalase and peroxidase activity to a similar extent by decreasing the rate of compound I formation (*7*, *9*). Thus, the role of the distal His and Arg is to bind and polarize the hydrogen peroxide molecule in concert with the heme iron. The imidazole ring of the distal His acts as a proton acceptor from H_2O_2, while the Arg side chain stabilizes the charged intermediates. The redox intermediate compound I is formed which has the iron oxidized to $Fe^{4+} = O$ (oxyferryl species) and a second oxidation equivalent either as a porphyrin cation radical (*7*, *9*, *18*) or protein radical (see below).

Most interesting is the reaction between the formed redox intermediate compound I and the second hydrogen peroxide molecule. Three types of heme enzymes are capable of performing H_2O_2 oxidation at a reasonable rate, namely, monofunctional catalases, catalase-peroxidases, and chloroperoxidases, the latter exhibiting a catalatic activity not more than 2% of catalases and KatGs. These three groups differ in the active site architecture and the pH profile of the catalatic activity, indicating that they do not share the same mechanism of hydrogen peroxide oxidation (*19*). Classical monofunctional catalases are essentially pH-independent from pH 5 to 10 (*20*), whereas all so far investigated KatGs show a sharp pH optimum between pH 6 and 7 (*5*, *6*, *21*, *22*). The corresponding pH optimum of *Synechocystis* wild

type KatG is at pH 6.5 (Figure 3). In monofunctional catalases, there are only two active site residues in locations where they can influence the oxidation of H_2O_2, namely, a histidine and an asparagine and a mechanism for compound I reduction in catalases was proposed by Fita and Rossmann (*24*) involving these two residues. Inspection of the active site in KatGs (Figure 1A) show that principally four residues could be involved in binding hydrogen peroxide to compound I, namely, Arg119, Trp122, His123, and Asp152. A recent analysis of the role of distal His, Arg, and Trp in *E. coli* (*7*) and *Synechocystis* (*8*) KatG has shown that both His and Arg do not participate in compound I reduction. This was concluded from the findings that mutation of His123 and Arg119 as well as of Asn153, the hydrogen-bonding partner of His123 in *Synechocystis* KatG (Figure 1A), did not alter the ratio of rates of compound I formation and reduction by H_2O_2 or the pH dependence of the catalase activity (*9*, *25*). Exchange of Asn153 lowered the basicity of His123 hampering mainly its function as acid−base catalyst in compound I formation (*25*). By contrast, removal of Trp105 in *E. coli* KatG (while not affecting compound I formation to the extent that compound I could be identified by absorbance and EPR spectrometry) significantly inhibited its subsequent reduction by hydrogen peroxide (*7*). Similarly, exchange of Trp122 in *Synechocystis* KatG completely inhibited compound I reduction by hydrogen peroxide.

In this work, we have reported (i) a dramatic effect of exchange of Asp152 on the overall catalase but not on the peroxidase activity, (ii) an only small effect on compound I formation but a substantial effect on the two-electron (but not one-electron) reduction of compound I, and, as a consequence, (iii) the possibility to monitor the H_2O_2-mediated compound I formation and to calculate the bimolecular rate constant for this reaction to be 7.5×10^6 M^{-1} s^{-1} at pH 7 and 15 °C, and, (iv) a dramatic effect of exchange of Asp152 on the pH profile of the overall catalase activity.

We conclude that the indole ring of Trp122 and the carboxylate group of Asp152 are involved in the oxidation of the second hydrogen peroxide molecule. The sharp maximum of catalase activity in KatGs and the postulated mechanism shown in Figure 7 require the Asp side chain to be in its carboxylate form and the indole moiety to be in its protonated form to guarantee optimum binding of H_2O_2. The reducing hydrogen peroxide initially forms hydrogen bonds with the aspartate side chain, the indole ring, and the oxyferryl oxygen (Figure 7).

In the postulated reaction scheme in Figure 7, two alternative doubly oxidized states representing KatG compound I are shown. A typical compound I species involving the oxyferryl species in combination with a porphyrin radical (species A in Figure 7) and a second species involving the iron(IV) center and a protein radical (species B in Figure 7). Species A is formed from ferric wild-type KatG by peracetic acid as well as from the Trp122 and Asp152 mutants by either peracetic acid or hydrogen peroxide. This is also suggested from the spectral features as well as rapid freeze-quench electron paramagnetic resonance experiments with *Mycobacterium tuberculosis* KatG compound I formed with peracetic acid (*7*, *8*, *18*). The present work supports that species A is part of the catalase and peroxidase cycle of the Asp152 variants, since, (i) in contrast to wild-type KatGs the compound I-typical hypochromicity at the Soret region could be also obtained with hydrogen peroxide, (ii) the dominating species during H_2O_2 degradation by the Asp152 exhibited this compound I-like spectrum (Figure 5), and (iii) the reactivity of this compound I was independent of the nature of peroxide used for its formation (Table 2).

In wild-type KatG or in Pro151Ala, the steady-state spectrum in the presence of hydrogen peroxide showed no sign of compound I (identified from the peracetic spectrum), which could be interpreted that the rate of compound I reduction (k_2) exceeds that of compound I formation. Nicholls et al. (*19*) postulated the existence of an alternative compound I state involving protein radical(s), which is supported by the findings that (i) compound I produced by peracetic acid was unaffected by addition of hydrogen peroxide (*5*, *9*), and, (ii) the unusual high-spin spectrum of KatG compound II (*8*, *12*, Figure 6A), which may also indicate a more stable protein radical than the usual ferryl state. On the basis of its important role in the catalatic activity, Trp122 could be a potential radical site (species B in Figure 7), though this is not proven by EPR spectroscopy until now.

It has been shown in a theoretical study on the redox chemistry of peroxides (*26*) that hydrogen peroxide acts preferably either as a two electron equivalent oxidizing agent by oxygen transfer or as a two electron equivalent reducing agent by hydride ion transfer coupled with proton transfer, because two electron transfer processes are energetically favorable (*26*, *27*). Peroxidatic mechanisms for ethanol oxidation by monofunctional catalase compound I were proposed (*23*) explaining the stereospecific transfer of a hydrogen from ethanol to the oxyferryl center as a hydride. Fita and Rossmann (*24*) have concluded that the catalytic mechanism for the reduction of compound I by H_2O_2 could be identical to the proposed peroxidatic mechanism. It has to be noted that in case of a pairwise movement of electrons (hydride transfer) the oxygen formed in the catalatic reaction would be singlet oxygen rather than normal triplet oxygen. Since singlet oxygen has been shown to inactivate enzymes including catalases (*27*, *28*), it would not make evolutionary sense to release singlet oxygen out of the heme pocket. On the other side, it must not leave its successor complex in the active site and could rapidly decay to triplet oxygen, but the mechanism and kinetics of quenching are unknown. An alternative mechanism was recently presented by Nicholls et al. (*19*). Hydrogen peroxide oxidation is thought to occur in two hydrogen transfer steps to the oxyferryl oxygen and to the imidazole ring. The latter hydrogen is then transferred to the $Fe^{4+}-OH$ intermediate forming water and triplet oxygen and regenerating the enzyme in its native state (*19*).

In case of catalase-peroxidases, the hydrogen peroxide binds to compound I forming hydrogen bonds with the oxyferryl oxygen, the indole ring of Trp and the Asp side chain (Figure 7). The electronegative aspartate easily extracts a proton from the peroxide enabling a hydride transfer to the oxyferryl oxygen, forming $Fe^{3+}-OH^-$ and quenching the porphyrin radical cation. The role of the Trp in this stage might be to stabilize the nascent singlet oxygen during reaction. Finally, the proton on the aspartate is transferred to the $Fe^{3+}-OH^-$ species producing water and the ferric protein (Figure 7, left pathway). Alternatively, H_2O_2 oxidation occurs in two one-electron transfer steps with the first reducing equivalent being transferred either to the protein radical or to the oxyferryl oxygen. Transfer of the second

reducing equivalent finally produces water, triplet oxygen, and the enzyme in its native state (Figure 7, right pathway). In case of KatG, it is unlikely that the electronegative aspartate plays a role similar to that of histidine in catalases and accepts a reducing equivalent during reaction. At the moment it is not clear—similar to monofunctional catalases—if H_2O_2 oxidation of KatGs occurs by hydride transfer or by transfer of two reducing equivalents to compound I.

Nevertheless, the important role of aspartate and tryptophan in the catalatic activity of KatGs is evident from this and earlier studies. As mentioned above, another heme-containing peroxidase, namely, chloroperoxidase from *Caldariomyces fumago*, exhibits also some catalase activity (*30*, *31*). Interestingly, this peroxidase, which has no homology with peroxidases of the plant peroxidase superfamily, has only one relevant residue at the distal side, namely, a glutamate (*30*). A role of this glutamate in the hydrogen peroxide oxidation was postulated (*31*). However, the catalase activity of chloroperoxidase is low compared with KatGs or monofunctional catalases. This suggests that an acidic amino acid alone on the distal side does not present the optimal site for effective hydrogen peroxide binding and oxidation. The distal His/Asn couple in catalases or the distal Trp/Asp couple in KatGs provides a much better enzymatic equipment for H_2O_2 oxidation.

ACKNOWLEDGMENT

We thank Prof. Peter Nicholls (Department of Biological Sciences of University of Essex, U.K.) and Prof. Peter Jones (Department of Chemistry of the University of Newcastle, U.K.) for a very helpful correspondence.

REFERENCES

1. Welinder, K. G. (1992) *Curr. Opin. Struct. Biol. 2*, 388−393.
2. Yamada, Y., Fujiwara, T., Sato, T., Igarashi, N., and Tanaka, N. (2002) *Nat. Struct. Biol. 9*, 691−695.
3. Welinder, K. G. (1991) *Biochim. Biophys. Acta 1080*, 215−220.
4. Obinger, C., Regelsberger, G., Strasser, G., Burner, U., and Peschek, G. A. (1997) *Biochem. Biophys. Res. Commun. 235*, 545−552.
5. Jakopitsch, C., Rüker, F., Regelsberger, G., Dockal, M., Peschek, G. A., and Obinger, C. (1999) *Biol. Chem. 380*, 1087−1096.
6. Engleder, M., Regelsberger, G., Jakopitsch, C., Furtmüller, P. G., Rüker, F., Peschek, G. A., and Obinger, C. (2000) *Biochimie 82*, 211−219.
7. Hillar, A., Peters, B., Pauls, R., Loboda, A., Zhang, H., Mauk, A. G., and Loewen P. C. (2000) *Biochemistry 39*, 5868−5875.
8. Regelsberger, G., Jakopitsch, C., Furtmüller, P. G., Rüker, F., Switala, J., Loewen, P. C., and Obinger C. (2001) *Biochem. Soc. Trans. 29*, 99−105.
9. Regelsberger, G., Jakopitsch, C., Rüker, F., Krois, D., Peschek, G. A., and Obinger, C. (2000) *J. Biol. Chem. 275*, 22854−22861.
10. Dunford, H. B. (1999) *Heme Peroxidases*, Wiley-VCH, New York.
11. Heering, H. A., Indiani, C., Regelsberger, G., Jakopitsch, C., Obinger, C., and Smulevich, G. (2002) *Biochemistry 41*, 9237−9247.
12. Jakopitsch, C., Regelsberger, G., Furtmüller, P. G., Rüker, F., Peschek, G. A., and Obinger, C. (2002) *J. Inorg. Biochem. 91*, 78−86.
13. Finzel, B. C., Poulos, T. L., and Kraut, J. J. (1984) *J. Biol. Chem. 259*, 13027−13036.
14. Patterson, W. R., and Poulos, T. L. (1995) *Biochemistry 34*, 4331−4341.
15. Smulevich, G., Miller, M. A., Kraut, J., and Spiro, T. G. (1991) *Biochemistry 30*, 9546−9558.
16. Howes, B. D., Rodriguez-Lopez, J. N., Smith, A. T., and Smulevich, G. (1997) *Biochemistry 36*, 1532−1543.
17. Poulos, T. L., and Kraut, J. (1980) *J. Biol. Chem. 255*, 8199−8205.
18. Chouchane, S., Girotto, S., Yu, S., and Magliozzo, R. S. (2002) *J. Biol. Chem. 277*, 42633−42638.
19. Nicholls, P., Fita, I., and Loewen, P. C. (2001) *Adv. Inorg. Chem. 51*, 51−106.
20. Goldberg, I., and Hochman, A. (1989) *Arch. Biochim. Biophys. 268*, 124−128.
21. Goldberg, I., and Hochman, A. (1991) *Biochim. Biophys. Acta 991*, 330−336.
22. Levy, E., Eyal, Z., and Hochman, A. (1992) *Arch. Biochim. Biophys. 296*, 321−327.
23. Schonbaum, G. R., and Chance, B. (1976) in *The Enzymes* (Boyer, P., Ed.) pp 363−408, Academic Press, New York.
24. Fita, I., and Rossmann, M. G. (1985) *J. Mol. Biol. 185*, 21−37.
25. Jakopitsch, C., Auer, M., Regelsberger, G., Jantschko, W., Furtmüller, P. G., Rüker, F., and Obinger, C. (2003) *Eur. J. Biochem. 270*, 1006−1013.
26. Jones, P., and Perkines, P. G. (1967) *Nature 215*, 129−132.
27. Jones, P., and Suggett, A. (1968) *Biochem. J. 110*, 621−629.
28. Lledias, F., Rangel, P., and Hansberg, W. (1998) *J. Biol. Chem. 273*, 10630−10637.
29. Kim, S. Y., Kwon, O. J., and Park, J. K. (2001) *Biochimie 83*, 437−444.
30. Thomas, J. A., Morris, D. R., and Hager, L. P. (1970) *J. Biol. Chem. 245*, 3129−3134.
31. Sundaramoorthy, M., Terner, J., and Poulos, T. L. (1995) *Structure 3*, 1367−1377.

BI026944D